Universiteit Utrecht

Opleiding Natuur- en Sterrenkunde

A Hybrid Approach to better understand Jet Quenching through Jet Substructure Observables in a Quark-Gluon Plasma

Bachelor Thesis

Joppe Koene Derk Swart

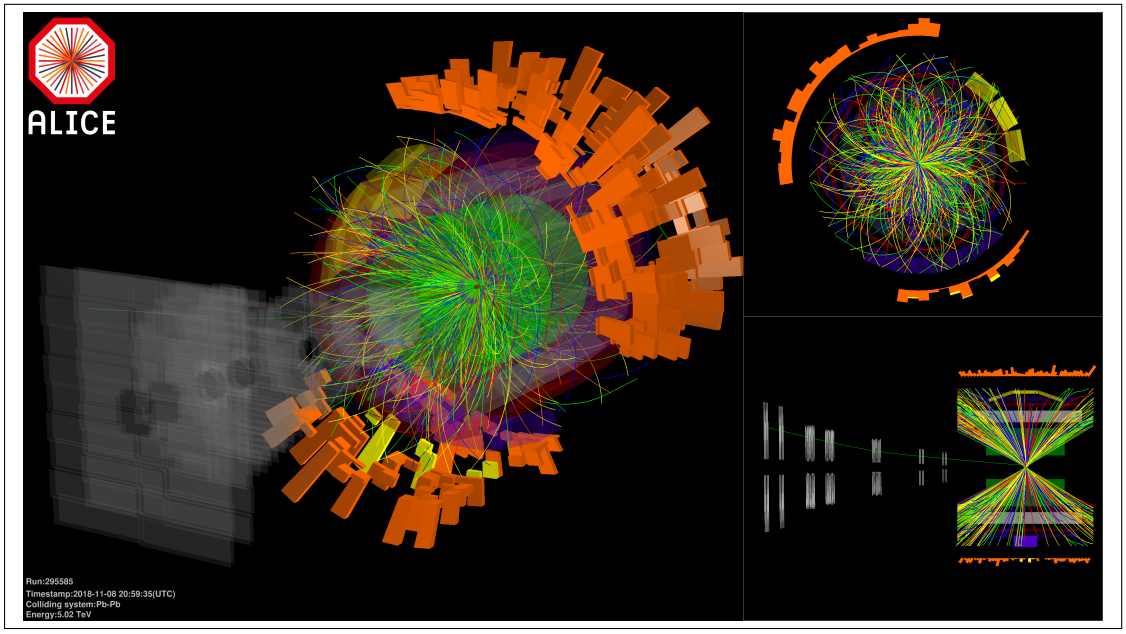

Supervisor:

Dr. Marta Verweij
Subatomic Physics

Abstract

In the last years, the interest in quark-gluon plasma has increased. In this thesis, we developed a way to better understand the QGP through an effect called jet quenching. We simulated two types of particle collisions. One with a Pythia sample that resembles hard scattering events in a vacuum and one with a Hybrid sample, that resembles hard scattering events in a QGP. With the production points of the jets from the Hybrid sample we made a selection for in- and outgoing jets at the edge of the QGP and outgoing jets produced near the centre. We compared four jet substructure observables in the different cases. We studied the way different observables were affected by the medium and in which case most jet quenching effects took place. We expected the outgoing jets from the Hybrid sample to look like the Pythia sample and the ingoing jets to undergo most jet quenching effects. We found that the ingoing jets from the Hybrid sample looked more like the Pythia results and the jets produced near the centre where the most quenched jets. The ingoing jets were not the most quenched since the cooling of the QGP was not taken into account.

Collision of Pb ions at LHC with energy of 5.02 TeV per nucleon pair recorded by ALICE on 08-11-2018. The colored lines represent the reconstructed trajectories of charged particles produced from the collision. The orange towers represent energy measured by electromagnetic calorimeters. Figure adapted from [1].

Contents

1 Introduction

Research on particle collision is of great scientific importance, not only does it allow us to study the fundamental forces of nature. It also allows us to get a better understanding of the universe just after the Big Bang [2]. The first few millionths of a second after the Big Bang, the universe consisted of a big soup completely build up from elementary particles, quarks and gluons. This soup is called a quark-gluon plasma, or short QGP. Although the Big Bang seems so mighty, we can create that same hot soup here on earth in one of the tiniest collisions imaginable. These collisions are performed in the Large Hadron Collider or LHC at CERN in Geneva Switzerland. When heavy ions collide at high energies a QGP is formed. In the LHC such heavy ions are accelerated near the speed of light and collide into each other. One experiment that is being conducted at CERN is A Large Ion Collider Experiment or short ALICE [3]. ALICE is designed to study the interactions of strongly interacting heavy ions and is specialized in the detection of QGP by detecting the effects on the particles.

A QGP can not be observed or measured. Instead, we need to look at other properties that happen during a collision to identify if a QGP is present. A powerful way to study the QGP is to look at the high energetic partons that are formed in the initial state of the collision. A shower of high energetic partons is formed. These partons interact with the QGP and loose energy due to interactions with the QGP, this process is called jet quenching. In the figure on the cover of this thesis the result of a Pb-Pb collision at the LHC, measured by ALICE is displayed. To get to such results, a lot of data analysis is needed. In this thesis, we will analyze simulations of such Pb-Pb collisions.

To get a better understanding of jet quenching and the QGP, we are going to look at four different jet substructure observables. We will look at these observables in different settings to determine the effect of jet quenching. We will use two different types of event samples to compare with each other. On the one hand, we study the Pythia sample (section 2.6.1), this sample represents a hard scatter in a vacuum. On the other hand, we study a Hybrid sample (section 2.6.2). This Hybrid sample includes a QGP where the partons interact with and the production points of the initial partons are given. This allows us to determine where the jets are produced and in which direction the jets go. The Pythia sample will be used as a reference system where no jet quenching has taken place. For the Hybrid sample, we will look at jets that are produced at the edge of the QGP and travel into the QGP, jets produced at the edge of the QGP that travel out of the QGP and jets produced near the centre of the QGP and travel out of the QGP.

The main question we ask ourselves is how jet quenching depends on the production point of the initial partons. We expect to find that the jets that are produced at the edge and travel out of the QGP, look the same as the Pythia results since both travel into a vacuum. Furthermore, we expect that the jets that travel into the QGP are quenched and have lost some energy due to the interactions with the QGP. We expect the jets that are produced near the centre to be less quenched than the jets that travel into the QGP and more quenched than the jets that travel out of the QGP from the edge.

2 Theory

2.1 The Large Hadron Collider

Let us first start by getting better knowledge of the detectors that measure particle collisions. Particle collisions happen in the Large Hadron Collider (LHC) at CERN. In the LHC, particles are accelerated up to the speed of light and then the particles are collided. The particles that travel through the LHC are accelerated with the help of powerful magnets. The magnets focus the particle beams and bend their trajectories. Since the LHC is a circular accelerator the particles can go as many rounds as needed to reach the speeds necessary for the collision. In each turn, the particles are given a bit more energy. The faster the particles go, the stronger the magnets need to be to accelerate the particles. The LHC is a 27 km long tube in which the particles can be accelerated [4].

There are several different experiments conducted at the LHC. In figure 1 one can see where the different experiments are located in the LHC. LHC-b, ALICE, ATLAS and CMS are the four experiments that are dedicated to the detection of heavy-ion collisions [5].

The ALICE detector is specialized in proving the presence of a QGP by looking at the particles produced in a collision [6]. Each of these experiments consist of a set of detectors that determine different properties of the collision. They detect the particles that are produced and look for instance at their momentum, mass and charge. All the detectors are built in layers around the detection point.

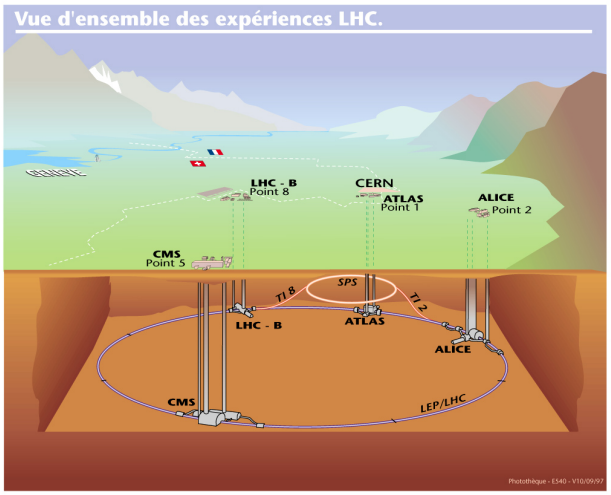

Figure 1: Overview of the Large Hadron Collider. Figure adapted from [7].

However, the samples and data that will be used in this thesis are not the real data retrieved from experiments at the LHC. The samples that are used are generated in such a way that they resemble a particle collision based on the results from the real data.

2.2 Jets

Jets are narrow cones of clustered particles produced in particle collisions. Jets are produced in a quantum chromo dynamic (QCD) hard scattering process. Two initial high momentum quarks or gluons (partons) are created and travel in opposite directions. In nature, single quarks can not be observed, they always come in the form of a hadron bounded by the strong interaction which is mediated by gluons. The two most known types of hadrons are mesons (pions, kaons) and baryons (protons, neutrons). Mesons consist of a quark and an antiquark and baryons consist of three quarks. One important property of quarks is their color charge, it has nothing to do with observable colors we know. The color charge is a quantum number

assigned to quarks. There are three colors: red, green and blue and respectively their anti-colors anti-red, anti-green and anti-blue. In nature, there is a restriction to the hadrons. every hadron has to be color neutral this is due to color confinement which will be explained later. For baryons, it means it should contain all three colors. For mesons, it means it should contain a color and the corresponding anti-color. There are six quarks: up, down, charm, strange, top, bottom. And their respective antiquarks having opposite charge and the anti-color. Due to the QCD confinement, these partons can not exist on there own since colorless states are the only states allowed.

Quarks are held together by the strong force which is carried by the gluon. Therefore, a gluon is also called a carrier of the strong force. The gluon falls in the category Gauge Bosons. Just as a quark, a gluon has a color but it is different from the color of the quarks. There are eight different color states in which a gluon can be. These states consist of a linear perturbation of different color and anti color pairs [8]. The colors are red, green, blue and their anti-colors. When quarks in a hadron are pulled away from each other, the gluon exerts a constant force to keep them together. Due to this, the quarks are confined within the hadron. It is energetically more favorable to generate a quark and antiquark pair than to split the bond between the quarks inside a hadron. This leads the initial partons to radiate of gluons or split into quark-antiquark pairs. These parton branch evolutions are governed by the QCD radiation probabilities given by Dokshitzer–Gribov–Lipatov–Altarelli–Parisi (DGLAP) equations [9] [10]. The DGLAP equations describe the branching of a parton shower in a vacuum. In a medium, we need to take some more branch evolution into account. In a QGP the initial partons suffer from soft exchange with the medium which alters the fragmentation pattern. The momenta transfer between the partons and the medium is small which leads to a strong coupling between the partons and the medium [11].

Due to color confinement, these partons can not exist on their own and need to make color-neutral hadrons. The process where quarks and gluons come together to form hadrons is called hadronization. Since more single partons are created for the initial parton to become color neutral, more partons are needed as long as all partons have hadronized and formed a color-neutral hadron. All these hadrons travel in the same direction, forming a cluster of particles better known as jets.

In this thesis, we will look at four different jet substructure observables produced in simulations. The observables we will look at are the thrust, width, multiplicity and p_T^D. The latter one is the momentum dispersion.

2.3 Quark Gluon Plasma

Quarks bind via the strong interaction, making it very hard to split them from each other. High temperatures and high densities are needed to do so. A few millionths of a second after the Big Bang the density and the temperature were high enough for quarks and gluons to exist in an unbound state, namely a Quark-Gluon Plasma (QGP).

To create a QGP, we need to reconstruct the extreme energies and densities at which a QGP occurs, this is done at CERN in the LHC. For the formation of a QGP, heavy-ion collisions are needed. Heavy ions like lead are accelerated up to the speed of light carrying energies up to 5.02 TeV per nucleon [12]. In figure 2 one can see how two lead ions collide. The blue and grey dots denote hadrons and the red dots denote QGP.

The energy of the collision creates enough heat to break the hadrons apart and make a QGP. Just after the collision there is a QGP but it quickly cools at a fraction $\frac{1}{time}$ and hadronization starts to happen (see section 2.2). The QGP is at the front of the collided ions. The lead ions have a head-on collision in the detector experiments, where all the properties of the collision are measured. The detector experiments look at how the energy, momentum and particle densities vary in different directions. In a collision, this is called flow. The elliptic flow is used to measure the uniformity of the flow when viewed in the azimuthal direction. The elliptic flow is the most important evidence for the existence of QGP. The collision of the two lead nuclei leads to a heating of the order of 10^{12}K. QGP can not be observed directly or with a microscope since it is very small and very hot and only exist for a fraction of a second before hadronization happens and the quarks and gluons stick back together to form color neutral states. It is needed to look at the results from the LHC experiments and simulations to get a better understanding of QGP.

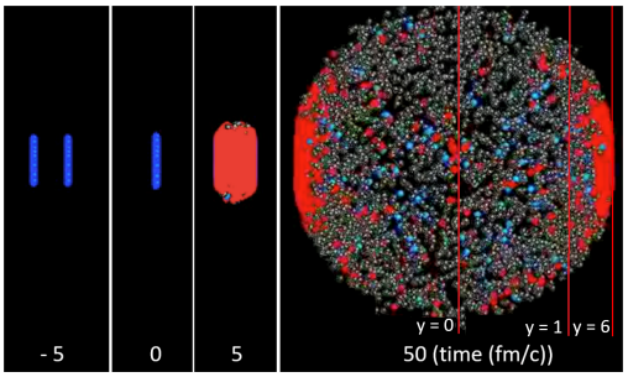

Figure 2: Formation of a QGP at different stages (white vertical lines) of a Pb-Pb collision with an energy of 2.76 TeV per nucleon. The time is given in fm/c. The blue and grey dots denote hadrons, and the red dots denote QGP. Figure adapted from [13].

2.4 Jet Quenching

To get a better understanding of QGP, it is needed to look at the properties of particles and particle jets that go through the QGP. QGP is a strongly coupled QCD medium. The partons that go through the QGP have strongly and weekly coupled interactions with the medium. In a head-on collision of heavy ions, particle jets are formed as described in section 2.2. Two colliding hadrons initiate an elastic or inelastic scattering of two partons. Which radiate gluons or split into quark-antiquark pairs that eventually ends up as a beam of particles. One of the clues for QGP formation was a phenomenon called jet quenching. In other words, the energy of jets weakened or the jets had disappeared at all. This was due to the fragmentation of a parton resulting from the energy loss to the QGP [9].

The strong coupled interactions between

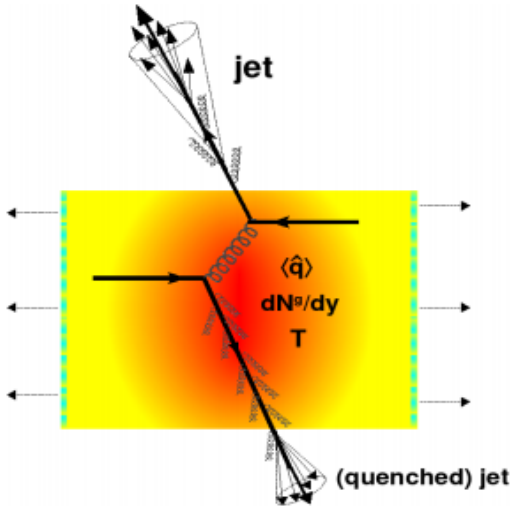

Figure 3: Schematic view of jet quenching in a QGP characterized by transport coefficient $\hat{q}$, temperature T and gluon density dN^g/dy. Figure adapted from [9].

a parton and the medium consist of a small momentum transfer from the parton to the QGP (see section 2.6.2).

In figure 3 one can see a schematic view of how jet quenching works for the weakly coupled interaction. In the figure, two partons are created in a hard scattering process after a head-on nucleus-nucleus collision. One parton travels directly into the vacuum where it radiates a few gluons before it hadronizes and forms a jet. The other parton travels into the QGP where it loses energy due to the radiation of gluons and has interactions with the QGP. Eventually, the jet hadronizes into a quenched jet. The energy loss due to a medium gives some fundamental information about the QGP. The energy loss depends on the properties of the medium (temperature T, particle medium interaction α, and thickness L) and the energy loss depends weakly on the properties of the initial parton (energy E and mass m). The energy loss can thus be characterized by $\Delta E(E, m, T, \alpha, L)$.

The following list of variables is taken from [9]. These variables are helpful in the characterization of energy loss in a medium:

- the mean free path $\lambda = \frac{1}{\rho\sigma}$, where ρ is the medium density ($\rho \propto T^3$ for an ideal gas) and σ the integrated cross-section of the particle–medium interaction,
- the Debye mass $m_D(T) \sim gT$ (where g is the coupling parameter). m_D characterizes the lowest momentum exchanges with the medium: the effective masses of the plasma constituents are $\mathcal{O}(m_D)$,
- the transport coefficient $\hat{q} \equiv m_D^2$ encodes 'the scattering power' of the medium through the average transverse momentum squared transferred to the traversing particle per unit path length. $\hat{q}$ combines both thermodynamical (m_D, ρ) and dynamical (σ) properties of the medium:
$$\hat{q} \equiv m_D^2 = m_D^2 \rho\sigma. \tag{1}$$
- the diffusion constant D, characterizing the dynamics of heavy non-relativistic particles (mass M and speed v) traversing the plasma, is connected, via the Einstein relations
$$D = 2T^2/\kappa = T/(M\eta_D) \tag{2}$$
to the momentum diffusion coefficient κ – the average momentum gained by the particle per unit time (related to the transport coefficient as $\kappa \approx \hat{q}v$) – and the momentum drag coefficient η_D.

There are two mechanisms for jet quenching due to weak coupled interactions in a QGP. The first one is collisional energy loss where partons have elastic scattering with one of the partons in the QGP. The average energy loss due to one elastic scattering with the medium is given by
$$\langle \Delta E_{coll}^{1scat} \rangle = \frac{1}{\sigma T} \int_{m_D^2}^{t_{max}} t \frac{d\sigma}{dt} dt. \tag{3}$$
Where $\frac{d\sigma}{dt}$ is the cross-section and t the momentum transfer. The collisional energy loss happens most of the time for particles with low momentum.

The second energy loss mechanism is the radiative energy loss. Radiative energy loss happens in the medium at high momenta per particle. The energy loss happens due to inelastic scattering of the initial parton. The energy loss can be characterized with the differential gluon bremsstrahlung spectrum ($\omega\frac{dI_{rad}}{d\omega}$ or $\omega\frac{d^2I_{rad}}{d\omega dk_\perp^2}$ where $\omega, k_\perp$ are the energy transverse momentum) [9]:

$$\langle \Delta E_{rad}^{1scat} \rangle = \int^E \omega \frac{dI_{rad}}{d\omega} d\omega \text{ or } \langle \Delta E_{rad}^{1scat} \rangle = \int^E \int^{k_T,max} \omega \frac{d^2 I_{rad}}{d\omega dk_\perp^2} d\omega dk_\perp^2. \tag{4}$$

The total energy loss of a jet is given by the sum of these two cases. $\Delta E^{tot} = N \times (\Delta E_{rad}^{1scat} + \Delta E_{coll}^{1scat})$ where $N = L/\lambda$ the opacity.

In figure 4 the two cases are drawn for a single scatter.

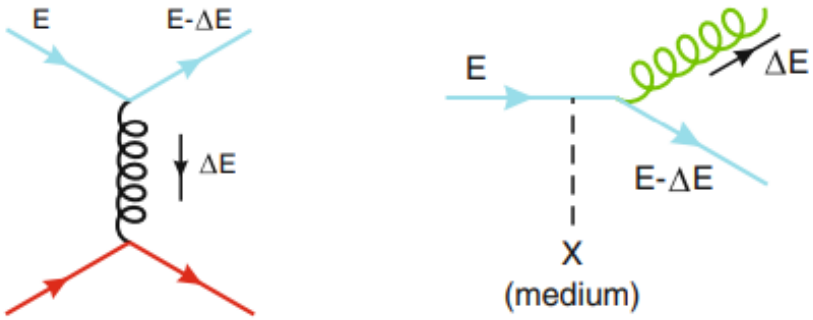

Figure 4: Diagrams of energy loss in a QGP. On he left the low momentum collisional energy loss and on the right, the high momentum radiative energy loss. Figure adapted from [9].

2.5 Heavy-Ions

The formation of a QGP is induced by heavy-ion collisions. The ions where we are interested in are lead ions. Two lead ions are accelerated to speeds near the speed of light in the LHC (see section 2.1). Due to the high speed, the theory of relativity needs to be taken into account. Due to Lorentz contraction, the nucleus can be interpreted as a Lorentz contracted disc with a diameter of 14 fm and a width of $\frac{14}{\gamma}$ fm. With $\gamma = \frac{1}{\sqrt{1-\frac{v^2}{c^2}}}$ the relativistic factor [13]. In the LHC this factor can reach a value of 2500 [13]. In the LHC two things can be set before the collision, namely what one collides and at what energies these collisions take place. The energies can be set very precisely but the quark content of the nucleons of the heavy ions that collide can only be interpreted as the average quark distribution in a nucleon. There also is no way to set the impact parameter that stands for the amount of overlap of the two colliding nuclei. For collisions, ions are needed instead of uncharged particles. Since ions are electrically charged one can accelerate them within a magnetic field as described in section 2.1. The reason we need heavy ions instead of single protons is that a single nucleon gains an amount of energy due to the acceleration. More nucleons in a collisions means more energy. In a proton-proton collision, there is not enough energy to create a QGP.

2.6 Simulation

We compare two different event samples with each other. we run over the Pythia sample, and the Hybrid sample. Most of the data analysis is done with a software toolkit called ROOT, designed by CERN for CERN experiments [14]. ROOT collects the data in a so-called tree, via the branches one can access the data easily. ROOT is a C++ based software package that has many properties for the visualization of data. To analyze and interpret the data, a framework to study the jet substructure in a heavy-ion environment was used, JetToyHI [15]. The software reads in the particle information takes care of mixing background with signal events.

2.6.1 The Pythia Sample

Pythia is a C++ based program used as a tool for the generation of high-energetic collisions using all the Standard Model physics as we know it. The particle generation is based on perturbative QCD describe in section 2.2. The DGLAP equations describe the evolution of the parton shower in the event. In the upper half of figure 5, a simplified version of such an evolution is displayed. Due to the high energies, the coupling strength α_s is small and thus allowing perturbative QCD [16]. In the Pythia sample, there are only weakly coupled interactions since there is no QGP.

Pythia generates a hard scattering process between a few body systems. It simulates all the interactions the particles have with each other. As a result, it gives a multi-particle system. Pythia 8.2 was used for the simulations.

Pythia simulates outgoing particles. The simulations do not take the interactions with detector material into account. Furthermore, the process happens in a vacuum with no QGP to interact with. Pythia allows for a lot of options to be set in a collision. Pythia generates both soft as hard QCD processes. In our simulations, we choose for hard QCD processes since that allows jet production above a minimum p_T. Below this p_T the Pythia results would not be reliable. The minimum p_T for a fixed target beam is 50 GeV [17].

Hadronisation in a Pythia event is based on the Lund string fragmentation framework [18]. For all the different physics components in Pythia, there are different parameters. These parameters are determined by the collaboration of theorists and experimentalists since some processes can not be predicted by perturbative theory alone. These parameters are collected in an option called tunes. In this thesis, we use option tune 14 [19].

When creating Pythia events, we give three options, the number of events, we used 100000. The tune, in our case 14 and an average momentum for the initial partons, the p_T-hat. In our case, we set the p_T-hat to 50 GeV.

The events are stored in a pu14 file. The data collected in the file is the 4-momentum vector and a so-called vertex number. The vertex number tells something about the identity of the particles. For the Pythia sample, there are two different particle identities. -1 denoting the initial partons and 0 denoting all the final-state particles produced as a result of the initial partons. There are two initial partons per event, traversing in opposite directions with the same initial momentum due to energy conservation.

In section 2.6.3 we go into more detail how these particles are clustered and form a jet.

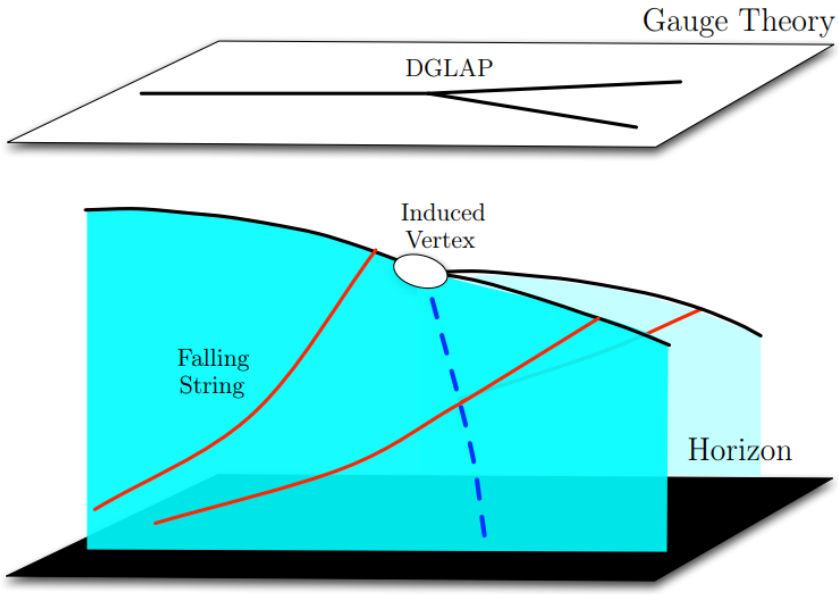

Figure 5: Sketch of two different methods to view the parton shower evolution. In the upper half is the parton evolution in a vacuum governed by the DGLAP equations. The lower half represents the evolution of a parton when both the strong and the weak coupling interactions are taken into account. Figure adapted from [11].

2.6.2 The Hybrid Sample

We compared the Pythia sample with the Hybrid sample. The main difference is that the Hybrid sample takes the QGP into account, this means that the initial partons and the jets formed from these partons undergo jet quenching. Another important difference between the Hybrid and the Pythia sample is that the initial partons in the Hybrid sample have a production point, allowing us to determine how much QGP the jets have traversed.

The Hybrid sample is based on different physics approaches that work on different energy levels. The Hybrid sample describes the change of the jets due to the QGP. The Hybrid sample takes the physics that describes jet production into account. In the Hybrid sample the QGP is considered strongly couples [11]. The Hybrid sample takes the energy exchange between the jets and the QGP into account.

To make the Hybrid sample work, a few assumptions are made. The splitting probability is unmodified by the QGP and thus the same as in the Pythia sample. The possibility of extra splitting induced by the exchanges of gluons with the medium is neglected.

The strongly coupled interaction between the medium and the partons is described by the Anti-de Sitter/conformal field theory correspondence. Or shortly, the AdS/CFT correspondence. The Hybrid sample describes the strongly coupled interactions between the QGP and the partons. In the lower half of figure 5 the idea of strong coupled interactions is drawn. The parton can be imagined as a particle with a string (red) that is attached to the particle and exchanges momentum with the QGP (black horizon plane). When the parton exchanges enough momentum it is being absorbed by the QGP since it does not have enough energy to travel further.

For a good representation of jet quenching, we need to know how much energy each parton loses to the QGP. The temperature of the QGP and the location of the interaction are needed to determine this. The momentum exchange between the QGP and the parton is in the order of the temperature of the QGP [11]. The momentum of the particles that are consumed by the QGP is used for the heating of the medium and results in more particles in the final state traversing in random directions. In gauge theory, the jets that traverse the QGP may suffer from hard splitting governed by the DGLAP equations [11].

We used a Hybrid sample with 100000 events. The sample represented a Pb-Pb collision with at least a 95% overlap of the colliding nuclei with an average p_T-hat of 50 GeV.

The pu14 file of the Hybrid sample is a bit different. It still contains the 4-momentum vector of each particle, but for the initial partons, there is an x and y production point given, the z component is 0 since it is a simulation at the moment of a collision in the z = 0 frame.

The Vertex numbers of the Hybrid samples are given by -2 for an initial parton, and 0 for a particle in the jets.

2.6.3 Jet Clustering and Jet Software

The Pythia and the Hybrid samples consist of events that in their turn consist of a lot of final state particles. The samples tell us nothing about the possible jets that can be observed. To see the jets, software is needed that makes a selection and cluster the particles traveling roughly the same direction into jets.

The jets are clustered by a C++ based software package called FastJet [20]

A jet is not necessarily an existing thing. It is a set of rules we gave to a bunch of particles to cluster them to study the properties of all the particles together. These rules are better known as jet algorithms. The properties of such clustered particles can tell us more about the initial parton in collider experiments.

The definition of a jet is done by a set of parameters and jet algorithms.

Most jets are formed by looking at the distance between the particles, if they are close enough they are joined. This is done over and over until a stopping condition is reached. These algorithms are called sequential recombination algorithms. The difference between different sequential jet algorithms are the stopping conditions and the choice of distance measure.

Another type of jet algorithms are cone algorithms. Cone algorithms put all the particles, in a specific angular region, together to form a jet. The momentum of such cones is measured by the sum of the momentum of each particle in the jet. The momentum of the jet is in the same direction as the cones axis. Hadronisation does not alter the direction of the energy of the parton, this results in stable cones being representative to real particles.

FastJet is mainly based on three longitudinally invariant sequential jet algorithms, namely the longitudinally invariant $k_\perp$ algorithm [21], the inclusive longitudinally invariant version of the Cambridge/Aachen jet-algorithm [22] and the inclusive anti-$k_\perp$ algorithm [23].

2.6.4 Jet Substructure Observables

To compare the jets of the unquenched Pythia sample and the quenched Hybrid sample, we need properties of the jets produced in the different samples. We look at four jet substructure

observables. These substructure observables are constructed with a component that depends on the momentum of the particles inside the jet and a component that depends on the azimuthal angle of the particles with respect to a certain axis. These observables are given by [24]:

$$\lambda_\beta^\kappa = \sum_{i \in jet} z_i^\kappa \left(\frac{R_i}{R_0}\right)^\beta . \tag{5}$$

These observables λ_β^κ are called generalized angularities, which depend only on angular component $\beta \geq 0$ and the energy weighting factor $\kappa \geq 0$. The observables are created by summing the product of z_i and $\frac{R_i}{R_0}$, where z_i is the momentum fraction of the particle, R_i is the azimuthal angle with respect to the axis of the jet and R_0 is the radius of the jet. Different values of κ and β give different observables. We focus on four different observables constructed with the values of β and κ as (β, κ). $(0, 0)$ is the particle multiplicity in the jet. $(0, 2)$ is the p_T^D, the momentum dispersion of the jets. $(1, 1)$ is the width of the jet and $(2, 1)$ give the thrust of the jet. One can choose other values for β and κ but they will not give insightful observables for the jet. In figure 6 the λ_β^κ space is drawn with the four observables. The line $(\beta, 1)$ represents the infrared and collinear (IRC) safe variables. For IRC safe angularities one can study the correlations between two observables analytically, for the IRC unsafe variables some techniques are needed to do so [24].

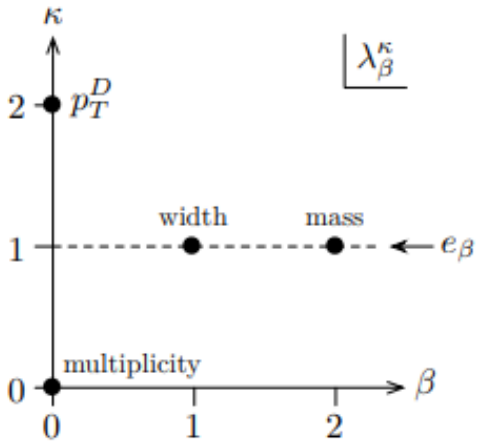

Figure 6: Visualisation of the space of observables λ_β^κ. Figure adapted from [24])

2.6.5 Jet Analysis

To represent the jet we use four jet substructure observables, created with the formula given in the previous section. The observables we found were the multiplicity, the width, the thrust and the p_T^D of the jet. But there are more properties to the jet that we are interested in to analyze our data. The jet substructure observables are stored in a tree called jetTree. In this jetTree, we have the properties of the initial partons and the jets that are created as a result of these partons. The different observables in the jetTree are calculated or subtracted from the data by the JetToyHI software.

The first thing which is calculated is the eventWeight. This is the number of initial partons of all the events. Thus, it is twice the number of events. Secondly, the observables for the initial partons are stored. The production points are extracted from the Hybrid data and stored in the tree, there are as many production points as there are events. The production points are called prodX and prodY in the jetTree. The next thing that is stored in the momentum of the partons called partonsPt. The momentum is calculated from the x-, y-, and z-component from the momentum that can be extracted from the data. To get

the total momentum, the following calculation is done: $p_T = \sqrt{p_x^2 + p_y^2 + p_z^2}$. With the momentum the direction of the initial partons can be determined. There are two directional observables. Namely the azimuthal angle (ϕ) around the collision, which is called partonsPhi. The angle goes from 0 to 2π radians. The other directional observable is the propagation in the direction along the beamline (η), this is called the partonsEta and it is measured from -1 fm to 1 fm. These two directional observables can be determined from the momentum of the partons. The next thing that is stored in the tree is the PDG code of the initial partons. In the jetTree, this is called partonPDG. The PDG code tells if the parton is a quark or a gluon. For the quarks, the number goes from 0 to 6 for quarks and from 0 to -6 for antiquarks. The PDG code for gluons is always 21. The PDG codes can be used to discriminate between the quark and the gluon jets. The next things that are stored in the tree are the properties of the jets that are produced by the initial partons. The first thing is the momentum of the jets. The total momentum of the jet is given by $\sum_{i \in jet} p_{T,i}$ where we sum over the momentum of all the final state particles. In the jetTree, the momentum of jets is called sigJetPt. Next up is the direction of the jets. The direction is determined by the main axis of the jet. The two directional observables for the jet are the same as the directional observables for the initial partons. The azimuthal angle (ϕ) lies between 0 and 2π radians and the distance along the beam direction (η) lies between -1 fm and 1 fm. For the jet, these observables are called respectively sigJetPhi and sigJetEta. Next up in the jetTree are the four jet substructure observables we are mainly interested in. The way these four jet substructure observables are calculated is described in section 2.6.4. For the p_T^D there is a more insightful calculation that writes out the momentum fraction:

$$p_T^D = \frac{\sqrt{\sum_{i \in jet} p_{T,i}^2}}{\sum_{i \in jet} p_{T,i}} [25]. \tag{6}$$

The jet substructure observables calculated in the previous section are called multiplicitySig which is a number, pTDSig which gives a ratio between 0 and 1, thrustSig which is in units of GeV/c^2 and widthSig which is in units of radians.

3 Method

Our main goal is to find the effects of jet quenching due to the amount of QGP that the initial partons travel through. Two samples are compared. The first sample is the Pythia sample, which resembles partons generated in the centre of a vacuum with no QGP, see section 2.6.1. This sample functions as a reference system for unquenched jets, produced at the edge of the QGP as in figure 3. The second sample is the Hybrid sample, where partons are generated in a QGP, see 2.6.2. This Hybrid sample has a specified production point in the xy-plane for each event. Both the samples consist of 100000 events. Each event consists of two initial partons that form two or more jets of final state particles, see section 2. The p_T-hat of both the samples was set to 50 GeV.

The first thing to do is to put a p_T cut on the events, this allows background noise to be filtered out. The Pythia and the Hybrid samples are both restricted to display the jets that appear in the $|\eta| < 1$ fm regime.

At first, we looked at the correlations between the four jet substructure observables found in section 2.6.4. For each event, a 2D histogram is drawn with the corresponding values of the correlation. The difference between the correlation of the Hybrid sample and the Pythia sample tells us what the average quenching effect is on the jet. To compare both the correlations, principle component analysis (PCA) was used on the correlations. PCA transforms a set of correlated variables into a set of uncorrelated values, called principle components. In appendix A.1, PCA is explained in more detail.

All the jet substructure observables in the Pythia sample were plotted in separate 1D histograms as reference for unquenched jets.

In the Hybrid sample, the production point of the initial partons is known. With this information, we can construct how much QGP the initial partons, and thus the jets, have traversed. The direction in which the partons go can be determined by the momentum and the angle (ϕ) of the initial parton (see section 2.6.5). We can construct a vector with a x-momentum and y-momentum component via:

$$p_{Tx} = p_T * \cos(\phi),$$
$$p_{Ty} = p_T * \sin(\phi).$$

Now we take the dot product with the vector from the origin to the production point and the vector we just calculated. In figure 7 a visualisation of the situation is given.

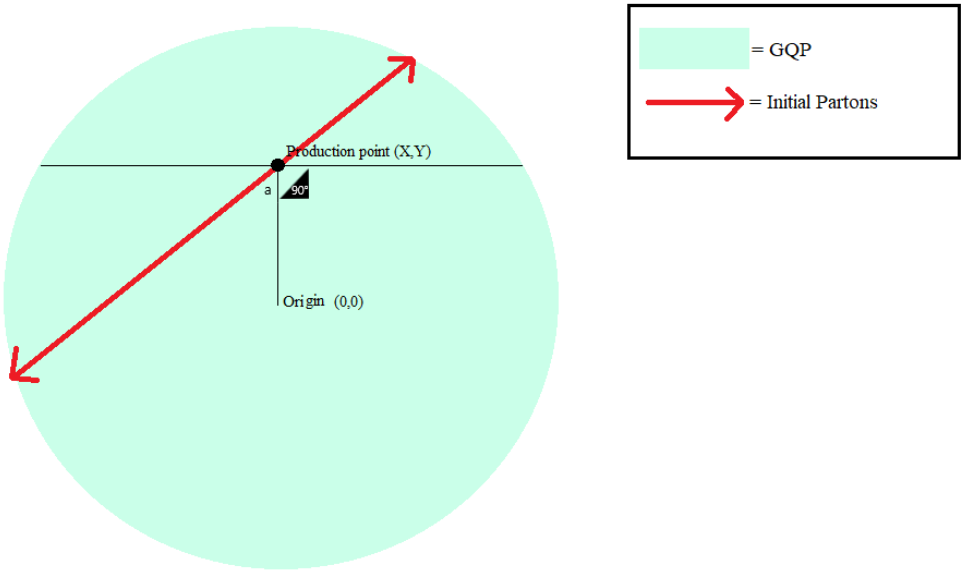

Figure 7: schematic overview of the production of two initial partons. Angle a is the angle between the direction of the initial parton and the vector from the origin to the production point.

The definition of the dot product is as follows:

$$\bar{v} \cdot \bar{w} = v_1 * w_1 + v_2 * w_2 = |\bar{v}| * |\bar{w}| * \cos(a),$$

where a is the angle between the two vectors. With the last definition of the dot product we can start to make a classification for the different cases. We make four different cases, namely $\cos(0°) = 1$, $\cos(90°) = 0$, $\cos(180°) = -1$ and $\cos(270°) = 0$. This means, that all the dot products that are positive, made an angle somewhere between $-90°$ and $90°$. In figure 7 that are all the lines one can draw above the black horizontal line. Since partons come in twofold and go the opposite direction, a positive dot product means that that parton traversed the least QGP of the two initial partons and thus had least jet quenching effects. But we are interested in the partons that traverse the most QGP. To find those jets we need to determine how far from the origin the production points are. The partons that traverse the most QGP are the ones produced at the edge of the QGP, and go straight at the origin, i.e. an angle of 180° and thus a negative dot product.

There is one special case, the one where the dot product is around 0. This means that the initial partons are produced at an angle perpendicular to the originvector. We can divide each jet parton into one of these four cases. The first case is a large dot product at the edge of the QGP. The second case is a large negative dot product at the edge of the QGP. The third case is a dot product around 0 at the edge. And the last one is everything produced near the origin. For every case, the four jet substructure observables will be drawn and the in- and outgoing jets will we compared with each other. Furthermore, every case will be compared to the Pythia jet substructure observables.

4 Results

The first thing to study is the difference in the correlation plots of the Pythia and the Hybrid samples. In the following results, we mainly focus on the principle component (PC), given as a red line, the second component (green line) is not significant unless stated otherwise.

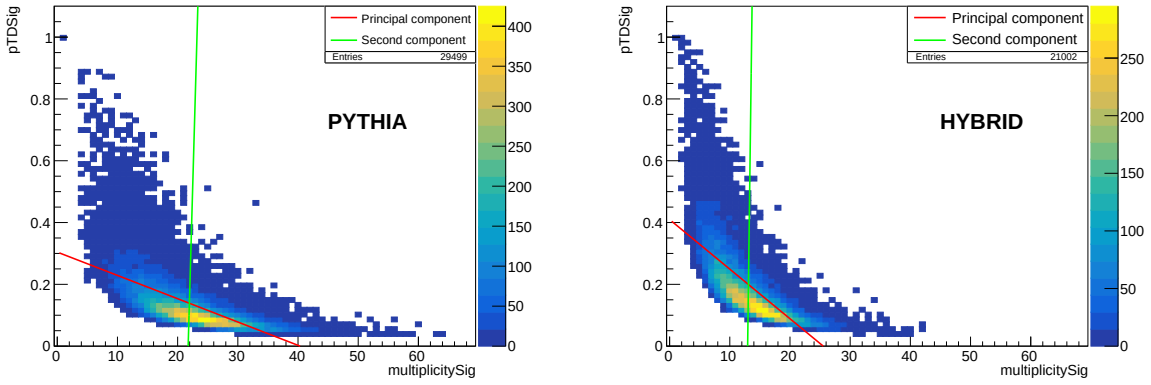

(a) The slope of the PC is −0.00754 with eigenvalue 54.429

(b) The slope of the PC is −0.0160 with eigenvalue 26.200

Figure 8: Multiplicity-p_T^D correlation. Figure 8a represents the Pythia results and figure 8b represents the Hybrid results.

In figure 8 the correlation between the multiplicity of the jets and the p_T^D of the jets is

presented. In both the figures, jets with a low multiplicity, have a high p_T^D. This is due to the definition of the p_T^D (see section 2.6.5). The fewer particles in a jet, the higher the p_T^D because the jet will be more collimated. The Pythia sample has roughly 10000 more entries. The Hybrid sample has fewer particles in their jets. The multiplicity of the Pythia sample stretches up to 65, where the Hybrid sample has a maximum of 45. The most correlated jets are with a relatively low p_T^D, around 0.1 and a multiplicity stretched from 20 to 30 for the Pythia sample, and 10 to 20 for the Hybrid sample. The slope of the PC of the Hybrid sample is 2.12 times steeper than the PC of the Pythia sample.

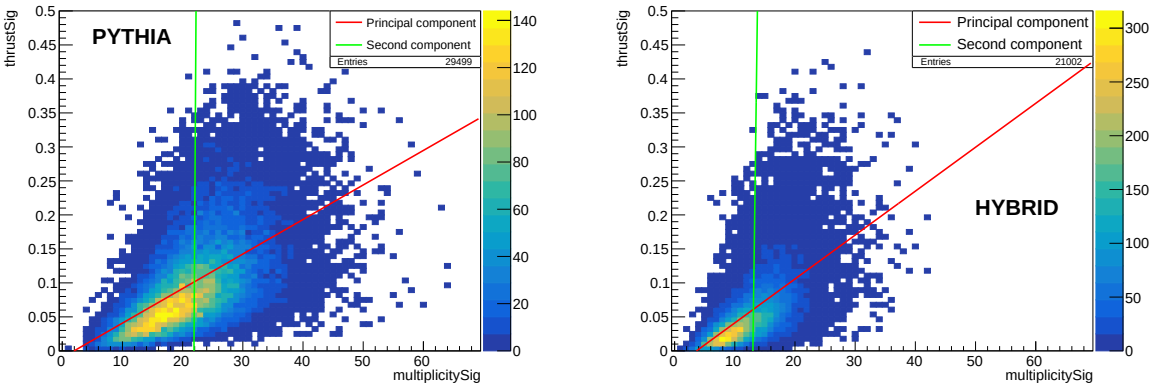

(a) The slope of the PC is 0.00508 with eigenvalue 54.427

(b) The slope of the PC is 0.00646 with eigenvalue 26.195

Figure 9: Multiplicity-thrust correlations. Figure 9a represents the Pythia results and figure 9b represents the Hybrid results.

In figure 9 the correlation for the multiplicity and the thrust of the jets is presented. One can see some linear correlation. Jets with higher multiplicity usually have a bigger thrust. This is due to the thrust of the single partons being added to form the thrust of the jet. The most correlated jets are in the region with a multiplicity from 10 to 30 and a thrust of 0.03 GeV/c^2 to 0.11 GeV/c^2 for the Pythia sample. For the Hybrid sample, the most correlated jets are with a multiplicity between 5 and 12 and a thrust between 0.01 GeV/c^2 and 0.05 GeV/c^2. The PC of the Hybrid sample is 1.272 times steeper than the Pythia sample.

In figure 10 the correlation between the multiplicity and the width is presented. One can see a linear correlation. Jets with a higher multiplicity, in general, have a bigger width. This is due to the sequential recombination algorithms. More particles in a jet mean more recombinations and thus wider jets. see section 2.6.3. The most correlated jets are in the region with multiplicity 10 to 30 and width between 0.08 rad and 0.3 rad for the Pythia sample. For the Hybrid sample, the most correlated values are in the region with multiplicity between 5 and 17 and width from 0.05 rad to 0.2 rad. The PC of the Hybrid sample is 1.470 times steeper than the PC of the Pythia sample.

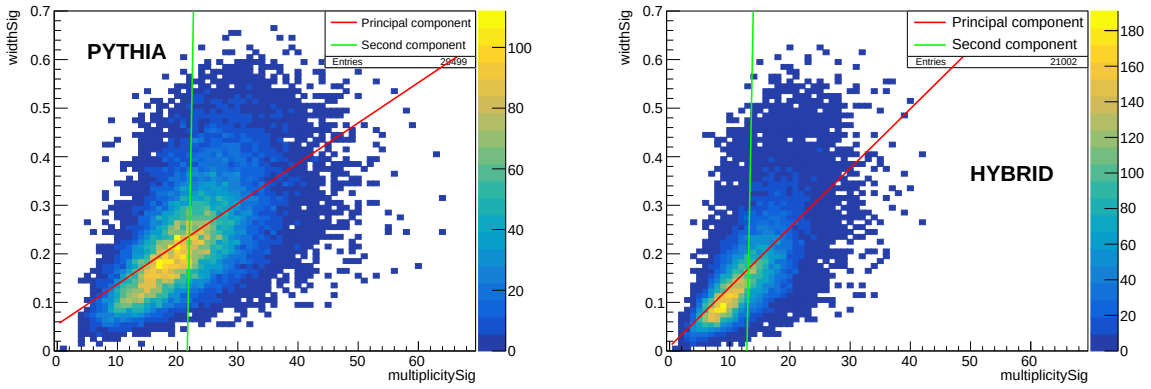

(a) The slope of the PC is 0.00830 with eigenvalue 54.430

(b) The slope of the PC is 0.0122 with eigenvalue 26.200

Figure 10: Multiplicity-width correlation. Figure 10a represents the Pythia results and figure 10b represents the Hybrid results.

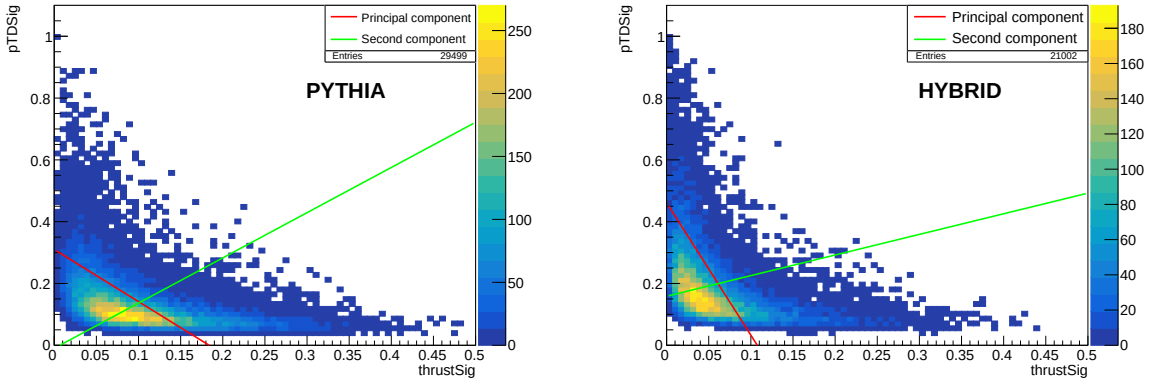

(a) The slope of the PC is −1.69 with eigenvalue 0.00867. The slope of the second component is 0.593 with eigenvalue 0.00290.

(b) The slope of the PC is −4.291 with eigenvalue 0.0147. The slope of the second component is 0.233 with eigenvalue 0.00225

Figure 11: Thrust-p_T^D correlation. Figure 11a represents the Pythia results and figure 11b represents the Hybrid results.

In figure 11 the correlation between the thrust and the p_T^D is presented. In the Pythia sample, it looks like most of the jets have a relatively low p_T^D whereas in the Hybrid sample the p_T^D is sightly higher on average. Jets that do not have as much thrust have a higher p_T^D. This is because jets with a low thrust have fewer particles in the jet, see figure 9. In the Pythia sample, most jets have a thrust between 0.03 GeV/c^2 and 0.15 GeV/c^2, and a p_T^D between the 0.05 and 0.175. For the Hybrid sample, the most correlated values are between a thrust of 0.01 GeV/c^2 and 0.1 GeV/c^2 and a p_T^D between 0.4 and 2.3. The eigenvalues for the second component are less than 10 times smaller. Thus they give reliable information

about the correlations. The slope of the PC of the Hybrid sample is 2.540 times steeper than the slope of the PC of the Pythia sample. The slope of the second component of the Hybrid sample is 0.456 times less steep than the second component of the Pythia sample.

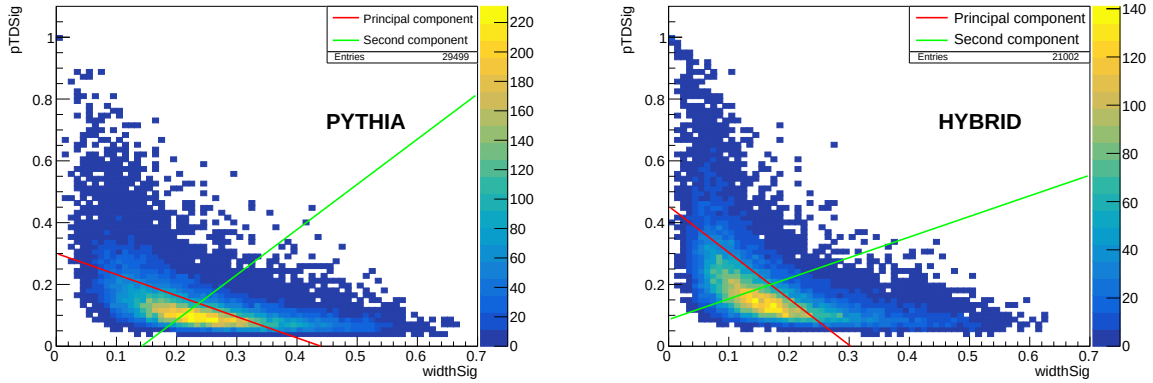

(a) The slope of the PC is −0.684 with eigenvalue 0.0140. The slope of the second component is 1.463 with eigenvalue 0.00397.

(b) The slope of the PC is −1.498 with eigenvalue 0.0181. The slope of the second component is 0.667 with eigenvalue 0.00505.

Figure 12: Width-p_T^D correlation. Figure 12a represents the Pythia results and figure 12b represents the Hybrid results.

In figure 12 the correlation between the width and the p_T^D is presented. For particles with a small width, the p_T^D is big. This is due to the multiplicity of jets with a small width, see figure 10. For jets with bigger width, the p_T^D is relatively small. Most of the jets in the Pythia sample have a width between 0.15 rad and 0.35 rad and a p_T^D between 0.05 and 0.15. In the Hybrid sample, most jets lie in the region with a width from 0.1 rad till 0.28 rad and p_T^D from 0.1 till 0.25. The slope of the PC of the Hybrid sample is 2.190 times steeper than the slope of the Pythia sample. The eigenvalues for the second component are less than 10 times smaller. Thus, they give reliable information about the correlations. The slope of the second component of the Hybrid sample is 0.393 times less steep than the slope of the second component of the Pythia sample.

In figure 13 the correlation between the width and the thrust is presented. Particles with small thrust have a small width and particles with a bigger thrust have a bigger width. For the Pythia sample, most jets lie in the region with a width from 0.1 rad to 0.3 rad and a thrust from 0.02 GeV/c^2 to 0.12 GeV/c^2. For the Hybrid sample, the width lies between the 0.05 rad and 0.17 rad. The thrust lies between 0.0 GeV/c^2 and 0.07 GeV/c^2. The slope of the PC of the Hybrid sample is not steeper than the slope of the PC of the Pythia sample. The slope of the PC of the Hybrid sample is 0.881 times less steep than the slope of the PC of the Pythia sample.

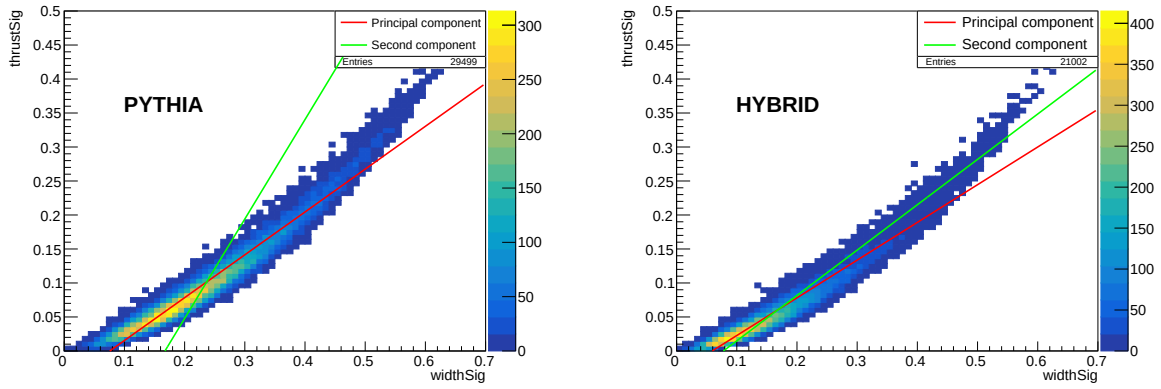

(a) The slope of the PC is 0.630 with eigenvalue 0.0150

(b) The slope of the PC is 0.555 with eigenvalue 0.0118

Figure 13: Width-thrust correlation. Figure 13a represents the Pythia results and figure 13b represents the Hybrid results.

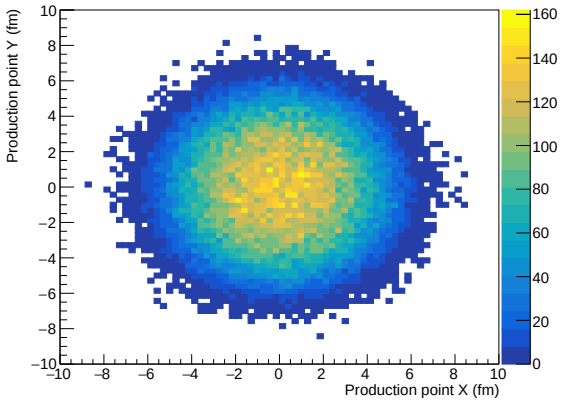

(a) Production points of the Hybrid sample

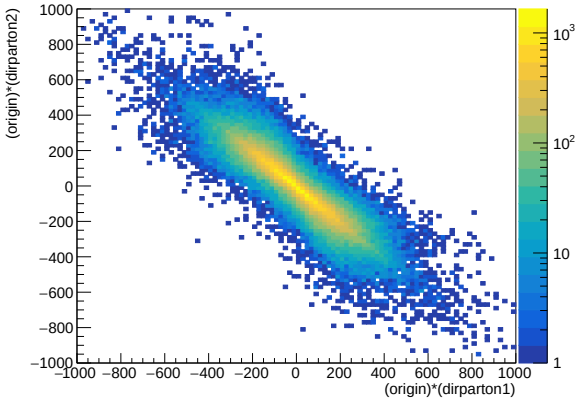

(b) Correlation from the dot products of the initial partons

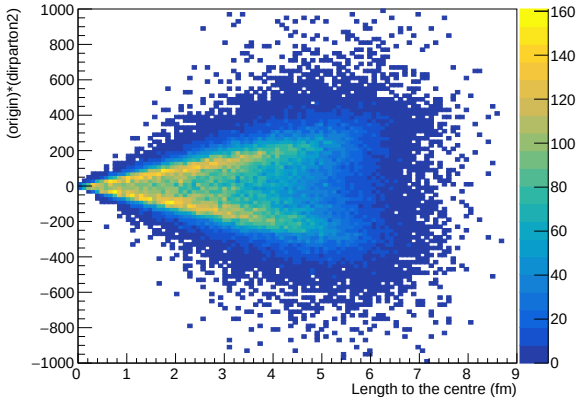

(c) Correlation between the length to the origin and the the dot products of one of the initial partons

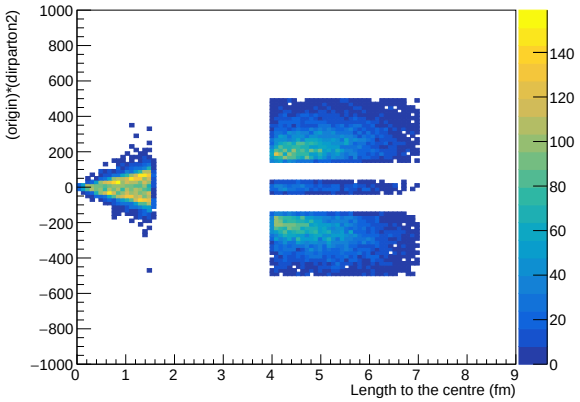

(d) Selected regions from figure 14c

Figure 14

In figure 14a the production points of the initial partons from the Hybrid sample are given. The particle density around the centre is the biggest. The production points range from -8 fm to 8 fm in both the $x-$ and the $y-$direction. From figure 14a we can calculate the dot products between the momentum vector of the initial parton and the vector from the origin to the production point as described in section 3.

In figure 14b the correlation between the dot products of the two initial partons is given. One can see that parton pairs that are produced far from the centre have one initial parton that has a large positive dot product, and the other initial parton has a large negative dot product. Most partons lie in the region with the dot product values between -400 and 400.

In figure 14c the correlation between the dot product and the length to the centre is given. Two lines stretch in the positive and the negative dot product direction. Figure 14c gives the correlation of one initial parton. The figure for the other initial parton looks similar. This is

because the production points are evenly distributed and that initial partons travel opposite directions. From figure 14c we selected the four regions of interest named in the section 3. In figure 14d these four regions are drawn. The first region is around the centre with all partons being produced within a radius of 1.5 fm. The next three regions are partons being produced in the outer ring from 4 fm to 7 fm. Here we make the distinction for outgoing partons (dot products between 150 and 500), ingoing partons (dot products between -150 and -500) and partons that go perpendicular with respect to the vector from the origin to the production point (dot products between 30 and -30).

The following results are divided into these four regions and compared with the Pythia sample. The four jet substructure observables from section 2.6.4 are plotted in each region.

In the Hybrid plots for the ingoing and outgoing jets, one can see how jet quenching alters the jet substructure observable.

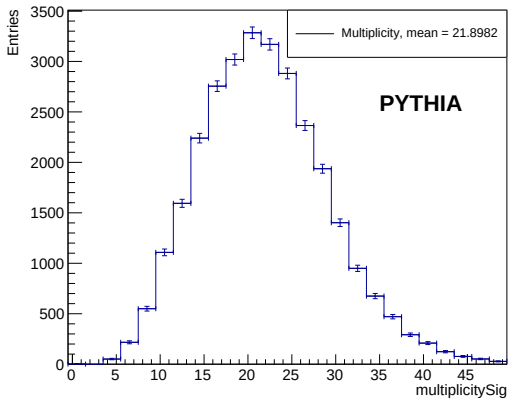

(a) Multiplicity of the jets in the Pythia sample

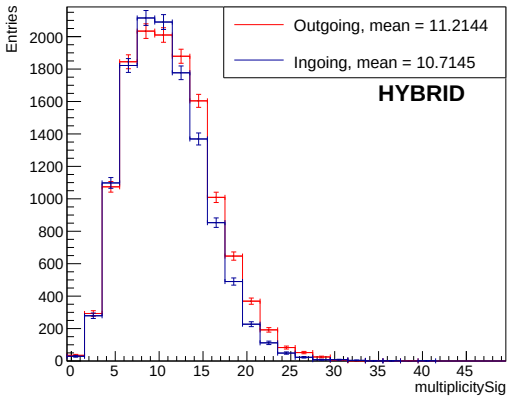

(b) Multiplicity for the ingoing and outgoing jets in the Hybrid sample. The outgoing jets have 13160 entries and the ingoing jets have 12356 entries.

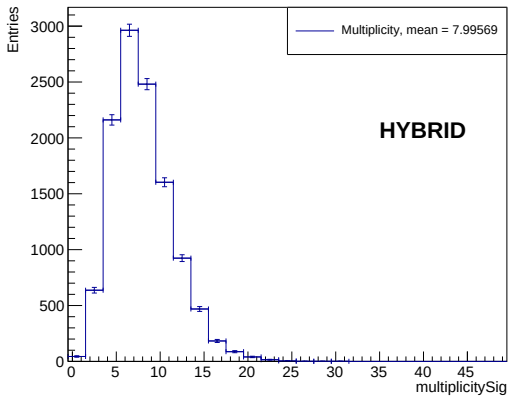

(c) Multiplicity for jets who are produced near the centre in the Hybrid sample

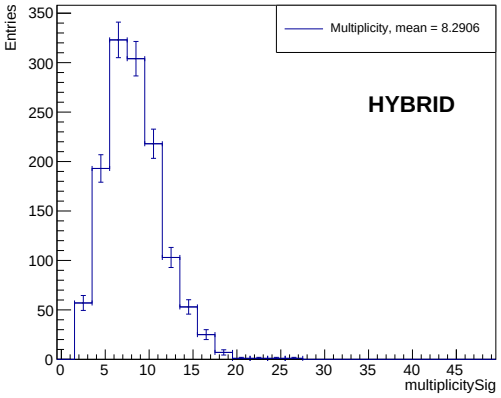

(d) Multiplicity of jets which are perpendicular with respect to the vector from the origin in the Hybrid sample

Figure 15: Histograms of jet multiplicities in different cases

In figure 15 the distribution for the multiplicity in the jets is presented. The first thing to notice is that the multiplicity in the Pythia sample in figure 15a is roughly twice as high as the multiplicity in the Hybrid sample. Therefore, it is hard to compare these two samples with each other in means of multiplicity. In figure 15b the multiplicity for jets that go in and out of the QGP is given. Jets that go into the QGP end up with a slightly lower multiplicity on average. Notice that for the bins in the region from 0 to 12 particles per jet, the ingoing jets have more entries. For the higher multiplicities, the outgoing jets have more entries. There are fewer entries for the ingoing jets due to jet quenching (see section 2.4) If we compare the jets that are produced at the edge of the QGP (figure 15b and 15d) and the jets produced at the centre (figure 15c), one can see that the jets at the edge, in general, have a higher

multiplicity than the jets produced near the centre. Figure 15c and figure 15d look familiar apart from the fact that the perpendicular jets have 10 times as less entries.

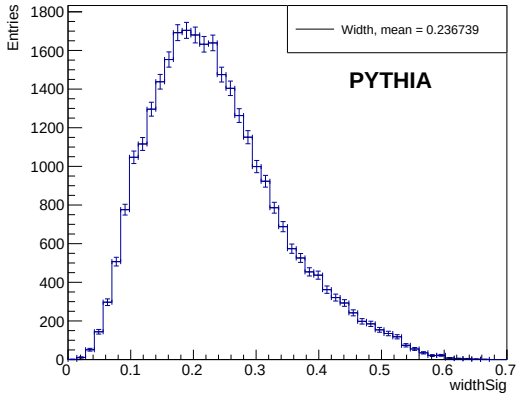

(a) Width of the jets in the Pythia sample

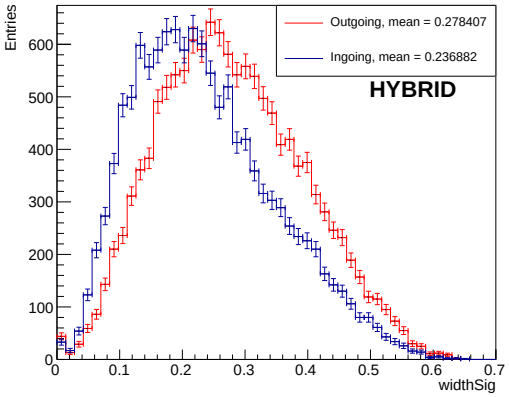

(b) Width for the ingoing and outgoing jets in the Hybrid sample.The outgoing jets have 13160 entries and the ingoing jets have 12356 entries.

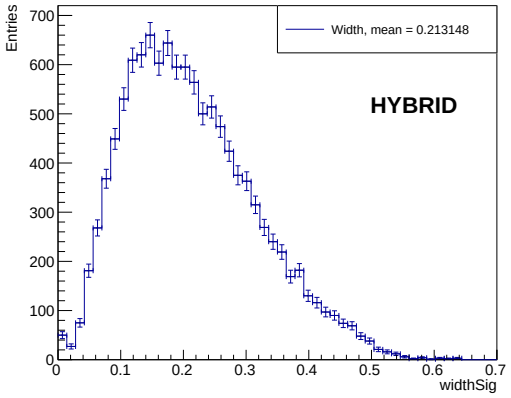

(c) Width for jets that are produced near the centre in the Hybrid sample

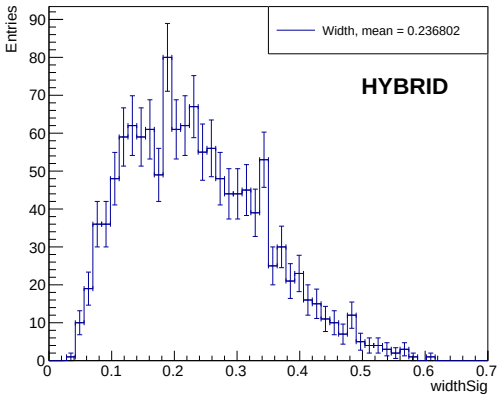

(d) Width of jets which are perpendicular with respect to the vector from the origin in the Hybrid sample

Figure 16: Histograms of jet widths in different cases

In figure 16 the different cases for the width of the jets are presented. In figure 16b one can see the width of the ingoing and the outgoing jets. The ingoing jets have a smaller width on average. One would expect the width of the outgoing jets to look like the Pythia sample in figure 16a, but in this case, the ingoing jet looks like the Pythia sample and have the same mean value. If we compare the jets which are created at the edge of the QGP (figure 16d, figure 16b) with the jets produced near the centre (figure 16c), we see that the jets near the centre have a smaller width. Figure 16d displays the jets that are perpendicular to the vector from the origin. There are 10 times less entries for the perpendicular case, which makes these

results less reliable.

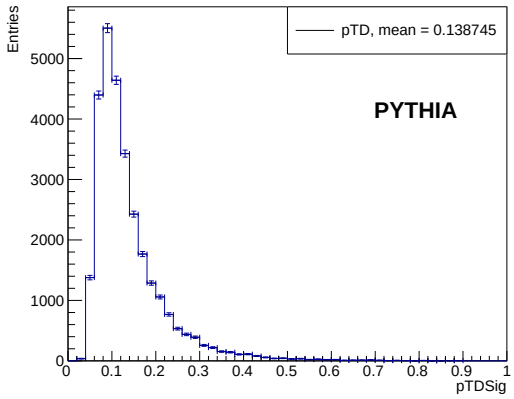

(a) p_T^D of the jets in the Pythia sample

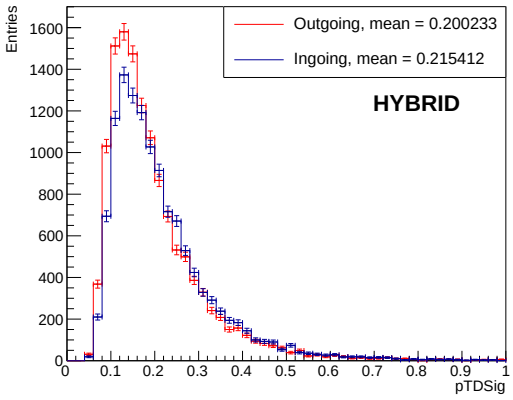

(b) p_T^D for the ingoing and outgoing jets in the Hybrid sample. The outgoing jets have 13160 entries and the ingoing jets have 12356 entries.

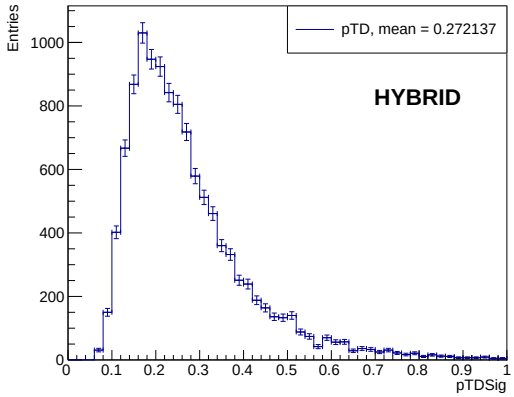

(c) p_T^D for jets which are produced near the centre in the Hybrid sample

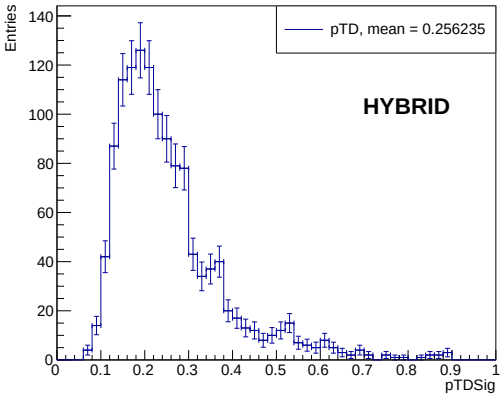

(d) p_T^D of jets who are perpendicular with respect to the vector from the origin in the Hybrid sample

Figure 17: Histograms of jet p_T^D in different cases

In figure 17 the distributions of the p_T^D is presented. In figure 17a one can see that the Pythia results for the p_T^D of the jets have a lower average p_T^D than any of the Hybrid results. This is a result of the higher multiplicity of the Pythia sample. In figure 17b the p_T^D of the ingoing and the outgoing jets is presented. One can see that the ingoing jets have fewer entries at the lower region p_T^D's. The mean of the ingoing jets is higher, which means there are fewer particles in the jet according to the definition of p_T^D in section 2.6.5. This is in accordance with the results found in figure 15b. The ingoing jets have fewer entries than the outgoing jets, this is an effect of jet quenching. When looking at the jets produced near the centre in figure 17c, one notices that the mean is higher than the mean for jets produced at the edge of the QGP. This is in accordance with the finding in figure 15c that there are fewer

particles in jets produced near the centre. The p_T^D of jets that go perpendicular to the vector from the origin look to be in between the jets produced at the edge and the jets produced at the centre when looking at the mean.

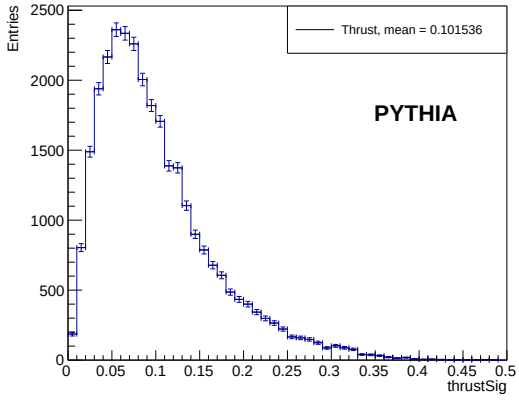

(a) Thrust of the jets in the Pythia sample

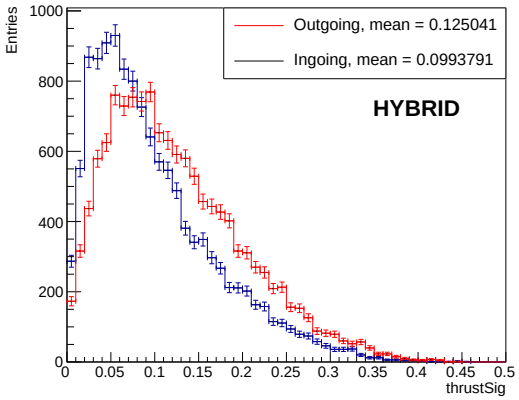

(b) Thrust for the ingoing and outgoing jets in the Hybrid sample. The outgoing jets have 13160 entries and the ingoing jets have 12356 entries.

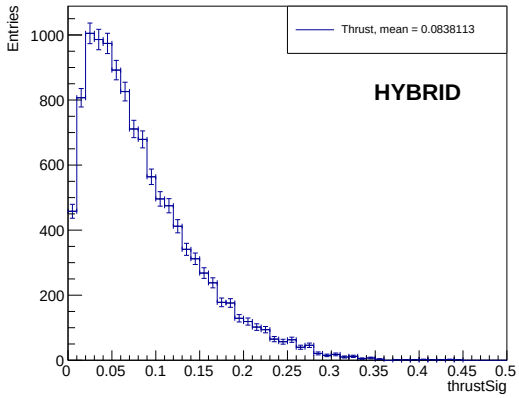

(c) Thrust for jets which are produced near the centre in the Hybrid sample

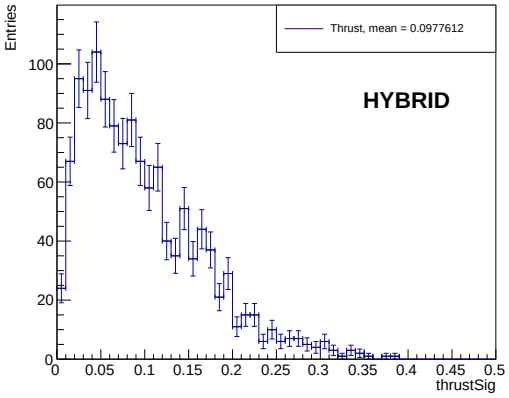

(d) Thrust of jets which are perpendicular with respect to the vector from the origin in the Hybrid sample

Figure 18: Histograms of jet thrust in different cases

In figure 18 the distribution of the thrust of the jets in different cases is presented. The Pythia sample in figure 18a and the Hybrid sample at the edge in figure 18b can not be compared since the mean in the Pythia sample is not the same as the mean of the thrust of the outgoing jets of the Hybrid sample. Instead, the Pythia thrust looks like the ingoing Hybrid thrust. In figure 18b one can see that for the ingoing jets the thrust is smaller with more entries in the lower region. The jets that are produced near the edge in figure 18c have a lower mean than the jets produced at the edge. This can be explained by figure 15c where

we see that there are fewer particles in jets produced near the centre. In figure 18d one can see that the thrust of the perpendicular jets has somewhat the same mean as the thrust of the outgoing jets and the thrust of the Pythia sample.

One can see that for all the observables, the ingoing jet has more entries than the outgoing jet.

5 Conclusion

We compared four different jet substructure observables with each other. We looked at two different particle samples. Namely the Pythia sample, that represented hard scatter in a vacuum. And the Hybrid sample, that represented hard scatter in a QGP. In the Hybrid sample, the production points of the initial partons are known. With the production points we made a selection of particles and calculated how much QGP was traversed by the jets. The selection of the Hybrid jets was as follows, we divided the jets into four categories: ingoing jets at the edge of the QGP, outgoing jets at the edge of the QGP, jets that go perpendicular with respect to the vector from the origin to the production point and jets that where produced in a radius of 1.5 fm around the origin. The edge of the QGP was taken from 4 fm to 7 fm.

The initial idea was to use the Pythia sample as a reference for the outgoing Hybrid jets that had little to no jet quenching. However, in section 4 it became clear that the Pythia results did not look like the unquenched outgoing jets from the Hybrid results. Instead, the observables for the ingoing jets had more in common with the Pythia results. We used four jet substructure observables to see the effects of jet quenching in the QGP. The main conclusions can be drawn from the comparison of the jet observables for the ingoing and the outgoing jets of the Hybrid sample.

For each observable, we found that there were fewer entries for the ingoing jets as for the outgoing jets. This is in accordance with our hypothesis and the observations done at CERN.

For the multiplicity, we found that the ingoing jets have more entries for the multiplicities between 0 and 12. For multiplicities above 12, the outgoing jets have more entries. This is because jets loose particles inside the QGP. The jets that went through the QGP lost some particles, making the entries at low multiplicity rise. Jets that are produced in the centre, in general, have a lower multiplicity than jets produced at the edge of the QGP.

For the width of the jet, we found that the ingoing jets in the Hybrid results had a lower width than the outgoing jets. This makes sense since there are fewer particles due to jet quenching. The Pythia results did not look like the outgoing Hybrid jets. The width of the Pythia jets looked more like the width of the ingoing Hybrid jets and even shared the same mean value. This may be because there are more entries in the Pythia sample. The width of the jets produced near the centre again has a lower minimum than the in or outgoing jets.

For the p_T^D we found that the ingoing jets in the Hybrid sample have a higher mean than the outgoing jets. This can be explained by looking at the definition of the p_T^D in section 2.6.5. Fewer particles due to jet quenching mean a bigger p_T^D. The Pythia result gives the lowest p_T^D. This is a result of the higher multiplicities in the Pythia jets. The p_T^D from jets generated near the centre on average has a higher p_T^D than the jets produced at the edge.

This means that there are fewer particles in the jets that are produced near the centre.

For the thrust, we found that the ingoing jets on average have a lower thrust than the outgoing jets. There are more entries in the low thrust region for the ingoing jets because the high thrust jets are quenched to lower thrust jets. The thrust of the Pythia jets looks like the thrust of the ingoing Hybrid jets. The jets produced near the centre on average have the lowest thrust.

For each observable, there was one remarkable thing. The hypothesis states that the ingoing jets undergo most jet quenching. From these results, we can conclude that jets produced near the centre undergo most jet quenching. This can be explained by the cooling of the medium, by the time the jets produced at the edge reach the centre, the QGP has cooled off so much that the density of the medium is a few times smaller than at the initial stage. The QGP expands and cools with $\frac{1}{time}$ as stated in section 2.3. Due to this cooling and the less dense medium, the jet quenching effects are less.

6 Discussion and Outlook

We tried to find how jet quenching did depend on the production point of the initial partons. To do so, we compared two different particle samples with each other. The Pythia sample and the Hybrid sample. We made a distinction between in- and outgoing jets that were produced at the edge of the QGP, jets produced near the centre of the QGP and jets that were perpendicular to the line from the centre to the production point. All these distinctions are made in the Hybrid sample. We expected the outgoing jets to be somewhat the same as the Pythia sample but we found that the Pythia sample looked more like the ingoing jets. For the thrust and the width, the Pythia sample looked more like the ingoing than the outgoing jets. The multiplicity and the p_T^D of the Pythia sample do not give reliable information to compare with the Hybrid sample since the multiplicity on average is higher in the Pythia sample.

We did find how all the different jet substructure observables interacted with the medium. We expected the jets that went into the QGP from the edge to be the most quenched case. But we found that the jets produced near the centre were most quenched. This is because the medium expands and cools and thus, being less interactive with the jets. The jets produced near the centre traveled through the high-density QGP and had more jet quenching than the ingoing jets.

For a next research, it is needed to make a better selection in both the Pythia and the Hybrid sample. Different cuts on the p_T can be studied to see the impact. The initial conditions for the Pythia and the Hybrid sample should be the same in every aspect except for the production points and the QGP in the Hybrid sample. There can also be a restriction on the angle at which the jets travel inside the QGP. Do they travel straight into the centre (180°) or are they shifted and pass the centre (eg. 135°).

The expansion and thus the cooling of the QGP should also be taken into account. There could be more precise regions, divided over the whole distance from the centre to the edge.

A bigger sample size is also preferable since we divide into different cases the error of our measurement rises and some results become unreliable.

7 References

References

[1] CERN. (2018). *First collisions of Pb ions in 2018 at the LHC recorded by ALICE.* Retrieved from http://cds.cern.ch/record/2646381/

[2] Nasa. (2019). *The Big Bang.* Retrieved from https://science.nasa.gov/astrophysics/focus-areas/what-powered-the-big-bang

[3] CERN. (2020). *ALICE.* Retrieved from https://home.cern/science/experiments/alice

[4] CERN. (2020). *Large Hadron Collider.* Retrieved from https://home.cern/science/accelerators

[5] Müller, B., Schukraft J., Wyslouch B. (2012). First Results from Pb+Pb collisions at the LHC. *Annual Review of Nuclear and Particle Science, 62.*
1-3 DOI: https://doi.org/10.1146/annurev-nucl-102711-094910

[6] ALICE. (2020). *ALICE.* Retrieved from http://alice.web.cern.ch/

[7] Caron, J. L. (1998). *Overall view of LHC experiments.* Retrieved from https://cds.cern.ch/record/841555

[8] Bottomley, J. Baez, J. (1996). *Why are there eight gluons and not nine?.* Retrieved from http://math.ucr.edu/home/baez/physics/ParticleAndNuclear/gluons.html

[9] d'Enterria, D. Betz, B. (2009). High-p_T Hadron Suppression and Jet Quenching. *The Physics of the Quark-Gluon Plasma.*
287-289. DOI: https://doi.org/10.1007/978-3-642-02286-9_9

[10] Paakkinen, P. (2015). *Dokshitzer–Gribov–Lipatov–Altarelli–Parisi evolution equations.* (Master's thesis). Retrieved from https://jyx.jyu.fi/bitstream/handle/123456789/48513/URN%3ANBN%3Afi%3Ajyu-201601281326.pdf?sequence=1isAllowed=y

[11] Casalderrey-Solana, J. Can Gulhan, D. Guilherme Milhano, J. Pablos, D. Rajagopal, K. (2014). A Hybrid Strong/Weak Coupling Approach to Jet Quenching. *Journal of High Energy Physics, 19.*
4-13. DOI: https://doi.org/10.1007/JHEP10(2014)019

[12] CERN. (2020). *Heavy ions and quark-gluon plasma.* Retrieved from https://home.cern/science/physics/heavy-ions-and-quark-gluon-plasma

[13] Busza, W. Rajagopal, K. van der Schee, W. (2018). Heavy Ion Collisions: The Big Picture, and the Big Questions. *Annual Review of Nuclear and Particle Science, 68.*
1-4. DOI: https://doi.org/10.1146/annurev-nucl-101917-020852

[14] ROOT. (2018). *About ROOT.* Retrieved from https://root.cern.ch/about-root

[15] Verweij, M. (2019). *JetToyHI.* Retrieved from https://github.com/mverwe/JetToyHI/tree/forbsc

[16] Gehrmann-De Ridder, A. (2013). *Pertubative QCD Lecture 1.* (PowerPoint presentation). Retrieved from https://indico.cern.ch/event/230448/attachments/381911/531283/CERN1.pdf

[17] Sjöstrand, T. Ask, S. Christiansen, J. R. Corke, R. Desai, N. Ilten, P. Mrenna, S. Prestel, S. Rasmussen, C. O. Skands, P. Z. (2014). An introduction to PYTHIA 8.2 *Computer Physics Communications,191.*
1-11. DOI: https://doi.org/10.1016/j.cpc.2015.01.024

[18] Andersson, B. Gustafson, G. Ingelman, G. Sjöstrand, T. (1983). Parton fragmentation and string dynamics. *Physics Report, 97.*
DOI: https://doi.org/10.1016/0370-1573(83)90080-7

[19] Skands, P. Carrazza, S. Rojo, J. (2014). Tuning PYTHIA 8.1: the Monash 2013 Tune. *The European Physical Journal, 74.*
DOI: https://doi.org/10.1140/epjc/s10052-014-3024-y

[20] Cacciari, M. Salam, G. P. Soyez, G. (2011). FastJet user manual. *The European Physical Journal, 72.*
1-8. DOI: https://doi.org/10.1140/epjc/s10052-012-1896-2

[21] Cantani, S. Dokshitzer, Yu. L. Seymour, M. H. Webber, B. R. (1993). Longitudinally-invariant $k_\perp$-clustering algorithms for hadron-hadron collisions. *Nuclear Physics B, 406.*
DOI: https://doi.org/10.1016/0550-3213(93)90166-M

[22] Atkin, R. (2015). Review of jet reconstruction algorithms. *Journal of Physics: Conference Series, 645.*
1-5. DOI: https://doi.org/10.1088/1742-6596/645/1/012008

[23] Cacciari, M. Salam, G. P. Soyez, G. (2008). The anti-k_t jet clustering algorithm. *Journal of High Energy Physics, 2008.*
1-4 DOI: https://doi.org/10.1088/1126-6708/2008/04/063

[24] Larkoski, A. J. Thaler, J. Waalewijnb, W. J. (2013). Gaining (mutual) information about quark/gluon discrimination. *Journal of High Energy Physics, 2014.*
1-4. DOI: https://doi.org/10.1007/JHEP11(2014)129

[25] Cunquerio, L. (2016). Jet shapes in pp and Pb–Pb collisions at ALICE. *Nuclear Physics A, 956.*
1-3. DOI: https://doi.org/10.1016/j.nuclphysa.2016.02.060

A Appendix

A.1 Principle Component Analysis

To analyze the correlations between the different jet substructure observables we used principle component analysis (PCA). PCA takes the patterns created by the correlations and gives a line of the most correlated values. We used PCA to compare the Pythia and the Hybrid correlations to see how they differ. The slope of the principle and the second component were compared to better understand what the most correlated values were.

The first thing we need to do for the PCA is to calculate the covariance matrix for each correlation. The definition of the covariance matrix is given below:

$$\begin{bmatrix} V_x & C_{x,y} \\ C_{y,x} & V_y \end{bmatrix}.$$

The matrix elements are determined in the following way, on the diagonal one sees the variance of one observable denoted by V_x. The covariance is denoted by $C_{x,y}$. The variance is calculated in the following way.

$$V_x = \frac{\sum(x_i - \bar{x})^2}{N}$$

where the sum is over all the x values in the dataset, $\bar{x}$ is the mean of x in the dataset and N is the total number of data points in the set. We divide by N to normalize the matrix.

The covariance is calculated in a slightly different way.

$$C_{x,y} = \frac{\sum(x_i - \bar{x})(y_i - \bar{y})}{N}.$$

N is still the number of data points in the dataset. Now we look at the correlation between the x- and y-values of the data set. $\bar{x}$ and $\bar{y}$ denote the mean x- and y-values of the dataset. If the variance and the covariance are calculated the covariance matrix can be filled.

Next up, is the calculation of the eigenvalues and corresponding eigenvectors of the covariance matrix. The eigenvalues are sorted from big to small. The bigger the eigenvalue, the more correlated the values. The eigenvector is the vector that points along the most correlated values. To construct a linear line that fits over our data we divide the y-component over the x-component of the eigenvector to get the slope of the line (s). Next up we shift this line by the mean values since our data set is not centreed around the origin. The principle component (PC) becomes:

$$PC = s(x - \bar{x}) + \bar{y}.$$

For the second component we do the same but we use the eigenvector corresponding to the second biggest eigenvalue.